Thermal Relaxation and Coherence Dynamics of Spin 3/2. II. Strong Radio-Frequency Field

JOHAN R.C. VAN DER MAAREL

Leiden Institute of Chemistry, Leiden University, Leiden, The Netherlands

ABSTRACT: The relaxation dynamics of the spin-3/2 density operator under strong, on-resonance radio-frequency (RF) irradiation and in the presence of fluctuating and static quadrupolar interactions is reviewed. The evolution under the lock is analyzed for any value of the static quadrupolar interaction, ranging from isotropic systems to systems exhibiting large splitting far exceeding the line widths. For isotropic systems, relaxation under off-resonance spin-locking conditions and in the multiple-pulse quadrupolar echo (QE) experiment is reviewed also. Spin-lock pulse sequences optimized for the selective detection of nuclei involved in slow molecular motion and/or in anisotropic, liquid crystalline environment are discussed. In Part I, the classical relaxation dynamics of spin 3/2 was reviewed.
 Concepts Magn Reson Part A 19A: 117–133, 2003

KEY WORDS: nuclear magnetic relaxation; quadrupolar nuclei; multiple-quantum spectroscopy; spin locking; quadrupolar polarization; multiple pulse; liquid crystal

INTRODUCTION

The magnetic relaxation of spin-3/2 quadrupolar probes (e.g., ^{7}Li, ^{23}Na, ^{39}K, ^{87}Rb, ^{35}Cl, ^{81}Br, and ^{131}Xe) provides a mechanism to extract information about molecular motions (*1*). Longitudinal relaxation gives information about relatively fast motions, whereas slow dynamics is probed by transverse relaxation through the spectral density of the fluctuating quadrupolar interaction at zero frequency. In part I of this series, the classical quadrupolar relaxation dynamics of spin 3/2 in the multipole basis was reviewed. In anisotropically oriented systems such as liquid crystals, the quadrupolar interaction may not be averaged completely to zero on the timescale of the inverse Larmor frequency and the spectrum displays a frequency splitting. For small splitting or if the satellites are spread out over a large frequency range, an accurate determination of the transverse relaxation rates becomes problematic and the slow dynamics is probed more efficiently by applying a lock through a strong radio-frequency (RF) field. The spin-lock experiment samples the spectral density at a frequency

Received 8 April 2003; revised 2 July 2003; accepted 2 July 2003

Correspondence to: Johan R.C. van der Maarel; E-mail: j.maarel@chem.leidenuniv.nl

Concepts in Magnetic Resonance Part A, Vol. 19A(2) 117–133 (2003)

Published online in Wiley InterScience (www.interscience.wiley.com). DOI 10.1002/cmr.a.10088

on the order of the RF strength. In previous works, it has revealed extremely slow ion dynamics on the order of tens of microseconds in dense Laponite clay suspensions (*2*) and the biopolymer Xanthan liquid crystal (*3*). Other motivations to consider the effects of relaxation during RF excitation originate from the increasing importance of sodium magnetic resonance imaging (MRI) in whole-body scanners (*4*) and the need to discern different pools (e.g., intracellular vs. intercellular) of ions in biological systems (*5*).

For a system of spin 3/2, the dynamics under a lock through an RF field can be solved in analytical form. As in part I, extensive use will be made of the irreducible tensor operators. First, I will review the spin-lock experiment and its variants pertaining to the isotropic environment. Here, the external (Zeeman and RF) parts of the Hamiltonian can be removed by a transformation to an interaction representation with a time-dependent Wigner rotation matrix. The advantage of this interaction representation is that it is relatively easy to show that the evolution of the spin system under locking conditions is similar to longitudinal relaxation in the rotating frame, but with modified rates. As an alternative to the spin-lock experiment, but with milder experimental constraints, the multiple quadrupolar echo (QE) experiment will be described. Then, I will move on to anisotropic systems and present the formalism to include the nonzero average, static quadrupolar interaction. In the presence of both an RF field and static quadrupolar interaction, the external Hamiltonian can not be removed by a simple transformation with a time-dependent Wigner transformation. Here, I will analyze first the time evolution of the density operator under the static Hamiltonian only. The effects of relaxation are treated subsequently as a first-order, time-independent, perturbation to the static Hamiltonian with a discrete spectrum of degenerate and nondegenerate eigenvalues (*6*). Finally, I will review a class of pulse sequences to extract information about the dynamics of the system of spin 3/2 subjected to the composed Hamiltonian. These pulse sequences include an additional coherence transfer pulse for selectively detecting nuclei (ions) in an anisotropic environment.

ISOTROPIC ENVIRONMENT

Spin-Locking Conditions

We consider a system of Larmor frequency ω_0 and we apply an RF field $B_1 = \omega_1/\gamma$ of frequency $\omega = \omega_0 - \Delta$, where γ is the gyromagnetic ratio. In the frame rotating at frequency ω, the effective field is the vector sum of the RF field and the offset $\omega_{\text{eff}} = (\omega_1^2 + \Delta^2)^{1/2}$ and makes an angle $\beta = \tan^{-1}(\omega_1/\Delta)$ with the direction of the Zeeman field. In the Larmor frequency–rotating frame, the static Hamiltonian $H_S^* = \Delta I_z + \omega_1 I_x$ does not commute with the fluctuating quadrupolar interaction $H_{QF}^*(t)$ and has to be included in the relaxation superoperator in Eq. [8] of Part I. The most convenient way to describe the time evolution of the spin system under locking conditions is to define an interaction representation in which the effective field disappears (*7, 8*). In the absence of a static quadrupolar interaction, this can be done by a transformation to the doubly rotating tilted frame (DRTF). In the DRTF, indicated by the double asterisk, the static Hamiltonian is removed and the master equation reads

$$d\sigma^{**}/dt = -\int_0^\infty \langle [H_{QF}^{**}(t), [H_{QF}^{**}(t-\tau), \sigma^{**}(t)]]\rangle d\tau \quad [1]$$

With the corresponding rank-two Wigner transformation matrix $D_{km}^{(2)}$ (with reduced elements $d_{km}^{(2)}$), the fluctuating, zero-average quadrupolar Hamiltonian is expressed as

$$H_{QF}^{**}(t) = C_Q \sum_{m,k=-2}^{2} (-1)^m T_{2k} D_{km}^{(2)} \times (-\omega_{\text{eff}} t, -\beta, -\omega t) F_{2-m}(t) \quad [2]$$

where the sign conventions and angle definitions of Rose are adopted (*9*). Restricting to the secular, non-oscillating terms, the expression of the time dependence of the density operator in terms of the spin operators takes on the form

$$\frac{d\sigma^{**}}{dt} = -\sum_{m=-2}^{2} [T_{2m}, [T_{2m}^{\dagger}, \sigma^{**}]] \sum_{k=-2}^{2} [d_{mk}^{(2)}(-\beta)]^2 \times (J_{mk}(m\omega_1 + k\omega) + iK_{mk}(m\omega_1 + k\omega)) \quad [3]$$

with the real and imaginary part of the spectral density

$$J_{mk}(m\omega_1 + k\omega) = (eQ/\hbar)^2 \text{Re} \int_0^\infty \langle F_{2k}^*(t) F_{2k}(t-\tau)\rangle \times \exp(i(m\omega_1 + k\omega)\tau) d\tau$$

$$K_{mk}(m\omega_1 + k\omega) = (eQ/\hbar)^2 \mathrm{Im} \int_0^\infty \langle F^*_{2k}(t) F_{2k}(t-\tau)\rangle \times \exp(i(m\omega_1 + k\omega)\tau) d\tau \quad [4]$$

respectively (*10*). Comparison of Eq. [3] here with Eq. [18] of Part I shows that the time evolution of the density operator and, hence, of the multipole operators in the DRTF are similar to that in the rotating frame but with spectral densities

$$\sum_{k=-2}^{2} [d^{(2)}_{mk}(-\beta)]^2 (J_{mk}(m\omega_1 + k\omega) + iK_{mk}(m\omega_1 + k\omega)) \quad \text{vs.} \quad J_m(m\omega_0) + iK_m(m\omega_0) \quad [5]$$

In the general case of off-resonance RF irradiation, coherences nonaligned with the effective field can be disregarded because they relax independently from the longitudinal components. Furthermore, these coherences are rapidly damped because of B_1 inhomogeneity and they can be separated from the spin polarization tensors by their precession frequency with respect to the spin-lock field. In the DRTF, the relevant longitudinal components are Zeeman order $\hat{T}_{10}$ and the spin polarization octopolar order $\hat{T}_{30}$, because rank-two quadrupolar order can not be created in an isotropic environment (see part I). Thus, the time evolution is similar to longitudinal relaxation (eigenstate population dynamics) in the rotating frame in Eq. [22] of part I:

$$\hat{T}_{10} \xrightarrow{R^{(\rho)}} \hat{T}_{10} f^{(\rho)}_{11}(t) + \hat{T}_{30} f^{(\rho)}_{31}(t)$$

$$\hat{T}_{30} \xrightarrow{R^{(\rho)}} \hat{T}_{30} f^{(\rho)}_{33}(t) + \hat{T}_{10} f^{(\rho)}_{13}(t) \quad [6]$$

with relaxation functions

$$f^{(\rho)}_{11} = 1/5[\exp(-R^{(\rho)}_1 t) + 4\exp(-R^{(\rho)}_2 t)]$$
$$f^{(\rho)}_{13} = f^{(\rho)}_{31} = 2/5[\exp(-R^{(\rho)}_1 t) - \exp(-R^{(\rho)}_2 t)]$$
$$f^{(\rho)}_{33} = 1/5[4\exp(-R^{(\rho)}_1 t) + \exp(-R^{(\rho)}_2 t)] \quad [7]$$

where the superscript (ρ) denotes dynamics in the presence of a lock through the RF field. To derive the relaxation rates, the spectral densities in Eq. [24] of part I have to be replaced by their counterparts in the DRTF according to Eq. [5]. Furthermore, the effective RF usually is much smaller than the Larmor frequency $\omega_{\mathrm{eff}} \ll \omega_0$ and, to a very good approximation, for $k \neq 0$ the spectral density function has the property $J_{mk}(m\omega_1 + k\omega) \approx J_k(k\omega) = J_{-k}(-k\omega)$. With the reduced Wigner rotation matrix elements (*9*), the expressions for the relaxation rates take the form

$$R^{(\rho)}_1 = 3/4\ \sin^2 2\beta J_{10}(\omega_{\mathrm{eff}}) + 1/2(2 + \cos 2\beta + \cos 4\beta)J_1 + 1/2(3 + \cos 2\beta)\sin^2\beta J_2$$
$$R^{(\rho)}_2 = 3/4\ \sin^4\beta J_{20}(2\omega_{\mathrm{eff}}) + 1/2(3 + \cos 2\beta)\sin^2\beta J_1 + 1/4(1 + 6\cos^2\beta + \cos^4\beta)J_2 \quad [8]$$

The rates contain the spectral densities at frequencies ω_{eff} and $2\omega_{\mathrm{eff}}$, respectively, and, hence, are sensitive to slow molecular motion. As in the case of longitudinal relaxation in the rotating frame, the relaxation under locking conditions is biexponential if the fluctuating quadrupolar interaction is outside the extreme narrowing limit.

After the spin-lock period, the B_1 field is switched off and the density operator has to be transformed back from the DRTF to the rotating frame. If the general form of the density operator in the DRTF is $\sigma^{**} = \sum_{l,m} c_{lm}\hat{T}_{lm}$, then in rotating frame the density operator is represented by $\sigma^* = \sum_{k,l,m} c_{lm}\hat{T}_{lk}D^{(l)}_{km}(0, \beta, \omega_{\mathrm{eff}}t)$. With the rotation properties in Table 2 of Part I, this change in interaction representation results in a transformation of the relevant tensor operators according to

$$\hat{T}_{10} \rightarrow \hat{T}_{10}\cos(\beta) + \hat{T}_{11}(a)\sin(\beta)$$
$$\hat{T}_{30} \rightarrow \hat{T}_{30}1/8(3\cos(\beta) + 5\cos(3\beta)) + \hat{T}_{31}(a)1/8\sqrt{3/2}(\sin(\beta) + 5\sin(3\beta)) + \hat{T}_{32}(s)1/2\sqrt{15}\cos(\beta)\sin^2(\beta) + \hat{T}_{33}(a)1/2\sqrt{5/2}\sin^3(\beta) \quad [9]$$

Depending on the frequency offset through the angle β, the created spin-polarization octopolar order $\hat{T}_{30}$ along the effective field transforms into single-, double-, and triple-quantum coherences. The multiple-quantum coherences can be monitored with the help of an additional coherence-transfer pulse at the end of the spin-lock period.

So far, the results are valid irrespective of frequency offset, which allows a broad range in effective field strength. However, it can be difficult to create an off-resonance RF irradiation, in the face of rapid relaxation, phase glitches, and carrier frequency switching (*11*). In the remaining part of this review,

we will deal exclusively with on-resonance RF irradiation. In the classical spin-lock experiment, the magnetization is initially transferred on the x-axis of the rotating frame in a $\hat{T}_{11}(a)$ state by a hard $(\pi/2)_y$ pulse followed by a spin-lock pulse with a 90° phase shift. In the DRTF, the magnetization is along the z-axis of the effective field and, hence, in this representation the density operator is expressed as $\sigma^{**} = \sqrt{5}\hat{T}_{10}$. The density operator now evolves according to Eq. [6] and, apart from the evolution into rank-one Zeeman order, spin-polarization octopolar order $\hat{T}_{30}$ is created

$$\sigma^{**}(t_1) = \sqrt{5}(\hat{T}_{10} f_{11}^{(\rho)}(t_1) + \hat{T}_{30} f_{31}^{(\rho)}(t_1)) \quad [10]$$

The evolution functions and rates are given by Eqs. [7] and [8], respectively. If the RF field is applied on resonance with $\omega = \omega_0$, $\omega_{\text{eff}} = \omega_1$, and $\beta = \pi/2$, the dependence of $R_1^{(\rho)}$ on $J_{10}(\omega_1)$ vanishes and the rates take the simplified form

$$R_1^{(\rho)} = J_1 + J_2 \quad R_2^{(\rho)} = 3/4 J_{20}(2\omega_1) + J_1 + 1/4 J_2 \quad [11]$$

Slow molecular motion is probed through the fast rate $R_2^{(\rho)}$, which contains the spectral density of the fluctuating quadrupolar interaction at two times the spin-lock frequency $2\omega_1$. Transforming back to the rotating frame according to Eq. [9], with $\beta = \pi/2$, the density operator represents a sum of single- and triple-quantum coherences

$$\sigma^{*}(t_1) = \sqrt{5}(\hat{T}_{11}(a) f_{11}^{(\rho)}(t_1) - 1/2\sqrt{3/2}\hat{T}_{31}(a) f_{31}^{(\rho)}(t_1) + 1/2\sqrt{5/2}\hat{T}_{33}(a) f_{31}^{(\rho)}(t_1)) \quad [12]$$

Under direct detection, the signal is proportional to the single-quantum coherence contribution and reads

$$s(t_1, t_2) = f_{11}^{(\rho)}(t_1) f_{11}^{(1)}(t_2) - 1/2\sqrt{3/2} f_{31}^{(\rho)}(t_1) f_{13}^{(1)}(t_2) \quad (T_{1\rho} \text{ relaxation}) \quad [13]$$

where the evolution functions during acquisition are given by Eq. [30] of part I. The second term on the right side of Eq. [13] comes from the rank-three single-quantum coherence, which evolves back into observable magnetization during the acquisition period. As in the case of the inversion recovery experiment, the effect of this interference term can be minimized by recording the amplitude of the detected signal immediately after the spin-lock pulse, or, alternatively, by integrating the entire spectrum after Fourier transformation of the free induction decay (FID).

According to Eq. [9], for $\beta = \pi/2$, the creation of the double-quantum coherence is suppressed, whereas the triple-quantum coherence contribution has maximum intensity. The triple-quantum coherence can be monitored with an additional coherence transfer pulse at the end of the evolution period

$$\pi/2(\phi) - B_1(\phi + 90),\ t_1 - \pi/2(0) - \text{acquire},\ t_2 \quad [14]$$

where the phase ϕ is stepped through the values 30, 90, 150, 210, 270, and 330°, while the receiver phase is toggled between 0 and 180° for consecutive scans. Another option to separate the different coherence orders is time-proportional phase incrementation (TPPI) of $\phi = n\Delta\phi$, with the counter $n = t_1/\Delta t_1$ and phase increment $\Delta\phi = 45°$ (*12*). TPPI has the advantage that all relevant coherences are monitored in a single experiment (see experimental example subsequently). It should be noticed that the filter contains a single transfer pulse only and not the conventional pulse pair at the end of the evolution period. It is not necessary to include a mixing pulse, because the multiple-quantum coherences are already excited during the evolution under the lock. With the transformation properties in Table 3 of part I, the single- ($p = 1$) and triple-quantum ($p = 3$) filtered signal contributions in the multiple-quantum filtered experiment with coherence transfer can be calculated and read, respectively,

$$s(t_1, t_2, p = 1) = f_{11}^{(\rho)}(t_1) f_{11}^{(1)}(t_2) + 1/8\sqrt{3/2} f_{31}^{(\rho)}(t_1) f_{13}^{(1)}(t_2)$$
$$s(t_1, t_2, p = 3) = -5/8\sqrt{3/2} f_{31}^{(\rho)}(t_1) f_{13}^{(1)}(t_2) \quad [15]$$

The spin-lock experiment essentially is two-dimensional (2D), either with or without coherence transfer. A set of spectra is obtained as a function of the spin-lock time t_1 after Fourier transformation with respect to the acquisition time t_2. A phase-sensitive 2D spectrum can be obtained by taking the real part of this set and subsequent Fourier transformation with respect to the evolution time t_1.

Multiple-Pulse QEs

The spin-lock experiment suffers from a number of experimental drawbacks. These drawbacks include the spectrometer time involved to acquire a full 2D

data set and the technical difficulties encountered in simultaneous switching of RF phase and power levels. In the Ostroff-Waugh multiple-pulse experiment, the continuous RF irradiation is replaced by a string of $(\pi/2)$ pulses (*13, 14*). The advantage is that the on-resonance, in-phase spin-echo amplitudes now can be sampled between the pulses and the relaxation curve can be recorded in a single scan. Furthermore, the pulse cycling time, which has a similar meaning as the RF power level in the continuous spin-lock experiment, can be varied easily in order to probe fluctuations with comparable correlation times.

In the pulsed experiment, the magnetization initially is transferred on the x-axis of the rotating frame in a $\hat{T}_{11}(a)$ state by a hard $(\pi/2)_y$ pulse followed by a sequence of $(\pi/2)_x$ pulses with cycling time T. Each pulse has duration τ_p with duty cycle parameter τ_p/T. Again, it is most convenient to define an interaction representation in which the (pulsed) RF field disappears (*7*). In the absence of a static quadrupolar interaction and with amplitude modulation only, this can be done by a transformation to the rotating tilted toggling frame (RTTF). In the RTTF, the effect of the amplitude-modulated RF irradiation on the fluctuating quadrupolar Hamiltonian is translated into a time-modulated argument of the Wigner transformation matrix

$$H^{**}_{QF}(t) = C_Q \sum_{m,k=-2}^{2} (-1)^m T_{2k} D^{(2)}_{km} \times \left(-\int_0^t \omega_1(t')dt', -\pi/2, -\omega_0 t \right) F_{2-m}(t) \quad [16]$$

Here, it is explicitly assumed that the RF field is applied on resonance. The time-dependent $\omega_1(t)$ is periodic in the cycle time T: $\omega_1(t) = \omega_1(nT + t_0)$, in which t_0 denotes the time elapsed after the nth echo. Restricting to the nonoscillating, secular terms, the differential equation for the *stroboscopically* sampled density operator takes on the form

$$\frac{d\sigma^{**}}{dt} = -\sum_{m=-2}^{2} [T_{2m}, [T^{\dagger}_{2m}, \sigma^{**}]] \times \sum_{k=-2}^{2} [d^{(2)}_{mk}(-\pi/2)]^2 J_{mk}(T, k\omega_0) \quad [17]$$

where the spectral density has been averaged over the cycle time

$$J_{mk}(T, k\omega_0) = (eQ/\hbar)^2 \frac{1}{T} \int_0^T \mathrm{Re} \int_0^{\infty} \langle F^{*}_{2k}(t) F_{2k}(t-\tau) \rangle \times \exp\left(i \left(m \int_{t_0-\tau}^{t_0} \omega_1(t')dt' + k\omega_0\tau \right) \right) d\tau dt_0 \quad [18]$$

Here, the imaginary part of the spectral density has been omitted, because in the relevant dynamics of the eigenstate populations (longitudinal relaxation) it vanishes anyway (see part I). The differential in Eq [17] describing the time evolution of the density operator in the RTTF is the same as that for continuous RF irradiation (Eq. [3]) but with pulse cycle time–dependent spectral density $J_{mk}(T, k\omega_0)$ vs. $J_{mk}(m\omega_1 + k\omega_0)$. This similarity is because the multiple pulses decouple the longitudinal subset $\hat{T}_{10}$ and $\hat{T}_{30}$ from any other coherence nonaligned with the pulsed RF field, like the effect of continuous RF irradiation in the spin-lock experiment (*14*).

In the limit of zero pulse spacing with duty cycle parameter $\tau_p/T \to 1$, one recovers the situation for the dynamics under locking conditions and $J_{mk}(T, k\omega_0)$ correctly reduces to $J_{mk}(m\omega_1 + k\omega_0)$. The average RF usually is much smaller than the Larmor frequency

$$m \frac{1}{\tau} \int_{t_0-\tau}^{t_0} \omega_1(t')dt' \ll k\omega_0, \quad k \neq 0 \quad [19]$$

and the integral over $\omega_1(t)$ in Eq. [18] can be neglected for $k \neq 0$: $J_{mk}(T, k\omega_0) \approx J_k(k\omega_0) = J_{-k}(-k\omega_0)$. The only important spectral density function to be evaluated is $J_{20}(T)$ $(k = 0)$. The other term with $k = 0$, i.e., $J_{10}(T)$, is irrelevant, because the dependence of the relevant relaxation rate $R_1^{(\mathrm{qet})}$ (see below) on $J_{10}(T)$ vanishes if the QEs are sampled on resonance. To calculate $J_{20}(T)$, we assume an exponential correlation function of the fluctuating quadrupolar interaction

$$\langle F^{*}_{20}(t) F_{20}(t-\tau) \rangle = A \exp(-\tau/\tau_c), \quad A = (2\pi\chi)^2/20 \quad [20]$$

with correlation time τ_c and χ denotes the root-mean-square coupling constant. The correlation function is sign modulated because of the effect of the $(\pi/2)$ pulse train and a pulse cycle time–dependent relaxation rate is observed if the cycle time is on the order

of the correlation time. The pulse cycle time–dependent expression of the spectral density function $J_{20}(T)$ takes on the form (*14*)

$$J_{20}(T) = A\tau_c\left(1 - \frac{\tau_p}{T}\left(\frac{(\pi\tau_c/\tau_p)^2}{1 + (\pi\tau_c/\tau_p)^2}\right)\right) - \frac{A\tau_c^2}{T}\left(\tanh\left(\frac{T}{2\tau_c}\right) + \frac{\sinh((T - 2\tau_p)/2\tau_c)}{\cosh(T/2\tau_c)}\right) \times \left(1 - \frac{2}{1 + (\pi\tau_c/\tau_p)^2} + \frac{1 - (\pi\tau_c/\tau_p)^2}{(1 + (\pi\tau_c/\tau_p)^2)^2}\right) \quad [21]$$

In the limit of δ − function pulses $\tau_p/T \rightarrow 0$, this expression can be simplified and reads

$$J_{20}(T) = A\tau_c\left(1 - \frac{2\tau_c}{T}\tanh\left(\frac{T}{2\tau_c}\right)\right) \quad [22]$$

and in the limit of zero pulse spacing, one recovers the expression for the experiment under continuous locking conditions

$$J_{20}(T = \tau_p) = \frac{A\tau_c}{1 + (\pi\tau_c/T)^2} = J_{20}(2\omega_1), \quad \omega_1 = \pi/2T \quad [23]$$

These two limiting expressions show a similar frequency behavior and are dependent on the cycle time T if T is on the order of the correlation time τ_c (*14*).

The time evolution of the stroboscopically sampled density operator in the multiple-pulse experiment is similar to that under continuous RF irradiation in Eq. [12]. If the in-phase and on-resonance QEs are sampled at echo times $t_n = nT$, the signal is proportional to the rank-one single-quantum coherence contribution

$$s(t_n) = f_{11}^{(\mathrm{qet})}(t_n) \quad \text{(QET experiment)}, \quad [24]$$

where the superscript (qet) has been used to discern the dynamics under the QE train (QET). The relaxation is a biexponential function

$$f_{11}^{(\mathrm{qet})}(t_n) = 1/5[\exp(-R_1^{(\mathrm{qet})}t_n) + 4\exp(-R_2^{(\mathrm{qet})}t_n)] \quad [25]$$

in which

$$R_1^{(\mathrm{qet})} = J_1 + J_2 \quad R_2^{(\mathrm{qet})} = 3/4J_{20}(T) + J_1 + 1/4J_2 \quad [26]$$

It should be noticed that the amplitude fraction of the slow and fast relaxing component is fixed to 0.2 and 0.8, respectively; there is no interference from the excited rank-three single-quantum coherence because of the sampling between the pulses.

As in the case of continuous RF irradiation, the excited triple-quantum coherence can be monitored with an additional coherence transfer pulse at the end of the pulse train

$$\pi/2(\phi) - [T/2 - \pi/2(\phi + 90) - T/2]_n - \pi/2(0) - \text{acquire}, t_2 \quad [27]$$

where the phase ϕ is stepped through the values 30, 90, 150, 210, 270, and 330°, with sign alternation of the receiver phase for consecutive scans. Another option is TPPI with $\phi = n\Delta\phi$ with the counter n and phase increment $\Delta\phi = 45°$. Analogous to Eq. [15], the single- and triple-quantum filtered signal contributions in the multiple-quantum filtered experiment with coherence transfer read, respectively,

$$s(t_1, t_2, p = 1) = f_{11}^{(\mathrm{qet})}(t_1)f_{11}^{(1)}(t_2) + 1/8\sqrt{3/2}\,f_{31}^{(\mathrm{qet})}(t_1)f_{13}^{(1)}(t_2)$$

$$s(t_n, t_2, p = 3) = 5/8\sqrt{3/2}\,f_{31}^{(\mathrm{qet})}(t_n)f_{13}^{(1)}(t_2) \quad [28]$$

with the biexponential relaxation function

$$f_{31}^{(\mathrm{qet})}(t_n) = 2/5[\exp(-R_1^{(\mathrm{qet})}t_n) - \exp(-R_2^{(\mathrm{qet})}t_n)] \quad [29]$$

Now, a true 2D experiment has to be done, in which the FID is acquired after the multiple-pulse sequence and the number of pulses n is incremented. It is clear that the experiment with coherence transfer is more time-consuming than the direct sampling method, but it has the advantage that signal from nuclei in the extreme narrowing limit does not contribute to the triple-quantum filtered signal.

Figure 1 shows a multiple-quantum spectrum of ^{23}Na in a poly-(methylacrylate) (PMA) ion exchange resin using the multiple-pulse sequence in Eq. [27] with TPPI (*14*). The spectrum represents a slice along F_1 at the resonance frequency in F_2. With a phase increment $\Delta\phi = 45°$ and a pulse cycle time $T = 60$ μs, the frequency shift between subsequent coherence orders takes the value $\Delta\phi/2\pi T = 2.08$ kHz. Hence, the feature at 2.08 kHz is the single-quantum contribution, whereas the signal at three times this frequency represents the triple-quantum filtered contribution [Fourier transform of $f_{31}^{(\rho)}(t_1)$]. Note that the

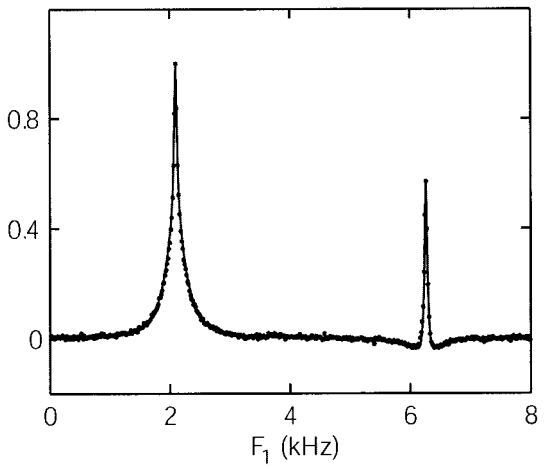

Figure 1 ^{23}Na multiple-quantum spectrum of a PMA ion exchange resin using the multiple-pulse QE sequence with TPPI. Experimental parameters: $\Delta\phi = 45°$, $T = 60$ μs, and $\tau_p = 10$ μs. The feature at 2.08 kHz is the single-quantum contribution, whereas the signal at three times this frequency represents the triple-quantum contribution; the double-quantum contribution is suppressed. The solid line represents a fit of the theoretical line shape as described in Ref. *14*.

double-quantum contribution is indeed suppressed, in accordance with Eq. [9] and for on-resonance conditions with $\beta = \pi/2$. If the RF irradiation is applied continuously, rather than pulsed, a very similar spectrum is observed (*15*). The line shapes agree with the theoretical predictions, but the relaxation rate of the fast relaxing component is not pulse cycle time dependent. In the PMA resin, the spectral density does not show dispersion in the low-frequency, kHz range and the rates agree with the spectral densities obtained with conventional relaxation experiments (*14*).

ANISOTROPIC ENVIRONMENT

In the *simultaneous* presence of a static quadrupolar interaction and an RF field, the external part of the Hamiltonian can not be removed by a relatively simple transformation to an interaction representation through a time-dependent Wigner transformation. In this situation, the static Hamiltonian $H_S^* = H_1^* + H_{QS}^*$ does not commute with the fluctuating quadrupolar Hamiltonian $H_{QF}^*(t)$ and has to be taken explicitly into account in the analysis of the relaxation contribution (*16–18*). Here, we will consider the on-resonance spin-lock experiment only. As far as I know, relaxation of spin 3/2 under off-resonance and/or pulsed RF irradiation and in the presence of a static quadrupolar interaction has not been treated in the literature. First, we will analyze the time dependence of the density operator under the static Hamiltonian only. The effects of relaxation will be treated subsequently as a first-order, time-independent, perturbation (*18*).

Unperturbed Time Dependence Under the Static Hamiltonian

In the multipole basis and without relaxation, the time evolution of the density operator under the static Hamiltonian

$$d\sigma^*/dt = -i[H_S^*, \sigma^*] = -i[\omega_1 T_{11}(a) + 1/\sqrt{6}\,\omega_Q T_{20}, \sigma^*] \quad [30]$$

reduces to two sets of differential equations. The first one is

$$\frac{d}{dt}\begin{pmatrix} \hat{T}_{11}(a) \\ \hat{T}_{20} \\ \hat{T}_{21}(s) \\ \hat{T}_{22}(s) \\ \hat{T}_{31}(a) \\ \hat{T}_{32}(a) \\ \hat{T}_{33}(a) \end{pmatrix} = \begin{pmatrix} 0 & 0 & i\sqrt{3/5}\omega_Q & 0 & 0 & 0 & 0 \\ 0 & 0 & -i\sqrt{3}\omega_1 & 0 & 0 & 0 & 0 \\ i\sqrt{3/5}\omega_Q & -i\sqrt{3}\omega_1 & 0 & -i\omega_1 & i\sqrt{2/5}\omega_Q & 0 & 0 \\ 0 & 0 & -i\omega_1 & 0 & 0 & i\omega_Q & 0 \\ 0 & 0 & i\sqrt{2/5}\omega_Q & 0 & 0 & -i\sqrt{5/2}\omega_1 & 0 \\ 0 & 0 & 0 & i\omega_Q & -i\sqrt{5/2}\omega_1 & 0 & -i\sqrt{3/2}\omega_1 \\ 0 & 0 & 0 & 0 & 0 & -i\sqrt{3/2}\omega_1 & 0 \end{pmatrix} \begin{pmatrix} \hat{T}_{11}(a) \\ \hat{T}_{20} \\ \hat{T}_{21}(s) \\ \hat{T}_{22}(s) \\ \hat{T}_{31}(a) \\ \hat{T}_{32}(a) \\ \hat{T}_{33}(a) \end{pmatrix} \quad [31]$$

and for the second set one has

$$\frac{d}{dt}\begin{pmatrix}\hat{T}_{10}\\ \hat{T}_{11}(s)\\ \hat{T}_{21}(a)\\ \hat{T}_{22}(a)\\ \hat{T}_{30}\\ \hat{T}_{31}(s)\\ \hat{T}_{32}(s)\\ \hat{T}_{33}(s)\end{pmatrix}=\begin{pmatrix}0 & -i\omega_1 & 0 & 0 & 0 & 0 & 0 & 0\\ -i\omega_1 & 0 & i\sqrt{3/5}\omega_Q & 0 & 0 & 0 & 0 & 0\\ 0 & i\sqrt{3/5}\omega_Q & 0 & -i\omega_1 & 0 & i\sqrt{2/5}\omega_Q & 0 & 0\\ 0 & 0 & -i\omega_1 & 0 & 0 & 0 & i\omega_Q & 0\\ 0 & 0 & 0 & 0 & 0 & -i\sqrt{6}\omega_1 & 0 & 0\\ 0 & 0 & i\sqrt{2/5}\omega_Q & 0 & -i\sqrt{6}\omega_1 & 0 & -i\sqrt{5/2}\omega_1 & 0\\ 0 & 0 & 0 & i\omega_Q & 0 & -i\sqrt{5/2}\omega_1 & 0 & -i\sqrt{3/2}\omega_1\\ 0 & 0 & 0 & 0 & 0 & 0 & -i\sqrt{3/2}\omega_1 & 0\end{pmatrix}\begin{pmatrix}\hat{T}_{10}\\ \hat{T}_{11}(s)\\ \hat{T}_{21}(a)\\ \hat{T}_{22}(a)\\ \hat{T}_{30}\\ \hat{T}_{31}(s)\\ \hat{T}_{32}(s)\\ \hat{T}_{33}(s)\end{pmatrix} \quad [32]$$

These two sets evolve independently, but they are coupled at a change of RF phase. On resonance, the matrices can be diagonalized and the differential equations can be integrated in analytical form (*19, 20*). The matrix in the first set has a 3D null space with three degenerate eigenvectors $\mathbf{A}_1$, $\mathbf{A}_2$, and $\mathbf{A}_3$ with eigenvalues $\lambda_0 = 0$ and four others $\mathbf{A}_{\pm 4}$, $\mathbf{A}_{\pm 5}$ with imaginary eigenvalues $\pm i\lambda_{1,2}$, being

$$\lambda_1 = \sqrt{\omega_Q^2 + 2\omega_1\omega_Q + 4\omega_1^2},$$
$$\lambda_2 = \sqrt{\omega_Q^2 - 2\omega_1\omega_Q + 4\omega_1^2} \quad [33]$$

whereas the matrix in the second set has eight eigenvectors with imaginary eigenvalues $\pm i\lambda_{3,4,5,6}$

$$\lambda_3 = \omega_1 + 1/\sqrt{2}\ \sqrt{\omega_Q^2 + 4\omega_1^2 + \lambda_1\lambda_2},$$
$$\lambda_4 = \omega_1 + 1/\sqrt{2}\ \sqrt{\omega_Q^2 + 4\omega_1^2 - \lambda_1\lambda_2}$$
$$\lambda_5 = \omega_1 - 1/\sqrt{2}\ \sqrt{\omega_Q^2 + 4\omega_1^2 + \lambda_1\lambda_2},$$
$$\lambda_6 = \omega_1 - 1/\sqrt{2}\ \sqrt{\omega_Q^2 + 4\omega_1^2 - \lambda_1\lambda_2} \quad [34]$$

The resulting time dependencies of the basis operators are rather complicated functions and have been set out by Campolieti et al. (*21*). Here, we will review those results only, which are of interest for the description of the evolution of the spin system under locking conditions.

In the on-resonance spin-lock experiment, the magnetization initially is transferred on the x-axis of

Table 1 Coefficients Giving the Time-Dependence of $\hat{T}_{11}(a)$ Under H_S^*

$a_{11}(t)$	$\frac{1}{10}\left[\frac{4(\omega_Q^4 + 4\omega_Q^2\omega_1^2 + 40\omega_1^4)}{\lambda_1^2\lambda_2^2} + 3\omega_Q^2\left(\frac{\cos\lambda_1 t}{\lambda_1^2} + \frac{\cos\lambda_2 t}{\lambda_2^2}\right)\right]$
$a_{20}(t)$	$\frac{3\omega_Q\omega_1}{2\sqrt{5}}\left(\frac{2(\omega_Q^2 + 4\omega_1^2)}{\lambda_1^2\lambda_2^2} - \frac{\cos\lambda_1 t}{\lambda_1^2} - \frac{\cos\lambda_2 t}{\lambda_2^2}\right)$
$a_{21}(t)$	$\frac{i\sqrt{3}\omega_Q}{2\sqrt{5}}\left(\frac{\sin\lambda_1 t}{\lambda_1} + \frac{\sin\lambda_2 t}{\lambda_2}\right)$
$a_{22}(t)$	$-\frac{\sqrt{3}\omega_Q}{2\sqrt{5}}\left[\frac{2\omega_1(\omega_Q^2 - 4\omega_1^2)}{\lambda_1^2\lambda_2^2} + \frac{(\omega_Q + \omega_1)\cos\lambda_1 t}{\lambda_1^2} - \frac{(\omega_Q - \omega_1)\cos\lambda_2 t}{\lambda_2^2}\right]$
$a_{31}(t)$	$-\frac{\sqrt{3}\omega_Q}{10\sqrt{2}}\left[\frac{4\omega_Q(\omega_Q^2 - \omega_1^2)}{\lambda_1^2\lambda_2^2} - \frac{(2\omega_Q + 5\omega_1)\cos\lambda_1 t}{\lambda_1^2} - \frac{(2\omega_Q - 5\omega_1)\cos\lambda_2 t}{\lambda_2^2}\right]$
$a_{32}(t)$	$-\frac{i\sqrt{3}\omega_Q}{\sqrt{5}}\left(\frac{\sin\lambda_1 t}{\lambda_1} - \frac{\sin\lambda_2 t}{\lambda_2}\right)$
$a_{33}(t)$	$\frac{3\omega_Q\omega_1}{2\sqrt{10}}\left(\frac{4\omega_Q\omega_1}{\lambda_1^2\lambda_2^2} + \frac{\cos\lambda_1 t}{\lambda_1^2} - \frac{\cos\lambda_2 t}{\lambda_2^2}\right)$

the rotating frame in a $\hat{T}_{11}(a)$ state by a hard $(\pi/2)_y$ preparation pulse, followed by a spin-lock pulse with a 90° phase shift. The first set of seven differential equations in Eq. [31] includes $\hat{T}_{11}(a)$ and, hence, is relevant for the description of the spin-lock experiment. It also includes $\hat{T}_{20}$, which is, as we will see, important for the calculation of the relaxation contribution. The eigenvalues and eigenvectors pertaining to the corresponding matrix are, respectively (*17*),

$$
\begin{aligned}
0 \quad \mathbf{A}_1 &= \sqrt{\frac{5}{2}}\frac{\omega_1^2}{\omega_Q^2}\hat{T}_{11}(a) + \sqrt{\frac{3}{2}}\frac{\omega_1}{\omega_Q}\hat{T}_{22}(s) + \hat{T}_{33}(a) \\
0 \quad \mathbf{A}_2 &= \left(\frac{5\omega_1^2}{\sqrt{6}\,\omega_Q^2} - \sqrt{\frac{2}{3}}\right)\hat{T}_{11}(a) + \sqrt{\frac{5}{2}}\frac{\omega_1}{\omega_Q}\hat{T}_{22}(s) + \hat{T}_{31}(a) \\
0 \quad \mathbf{A}_3 &= \sqrt{5}\frac{\omega_1}{\omega_Q}\hat{T}_{11}(a) + \hat{T}_{20} \\
\mp i\lambda_1 \quad \mathbf{A}_{\mp 4} &= \sqrt{\frac{2}{5}}\frac{\omega_Q}{\omega_1}\hat{T}_{11}(a) - \sqrt{2}\,\hat{T}_{20} \mp \sqrt{\frac{2}{3}}\frac{\lambda_1}{\omega_1}\hat{T}_{21}(s) - \sqrt{\frac{2}{3}}\left(1 + \frac{\omega_Q}{\omega_1}\right)\hat{T}_{22}(s) \\
&\quad + \frac{1}{\sqrt{15}}\left(5 + \frac{2\omega_Q}{\omega_1}\right)\hat{T}_{31}(a) \pm \sqrt{\frac{2}{3}}\frac{\lambda_1}{\omega_1}\hat{T}_{32}(a) + \hat{T}_{33}(a) \\
\mp i\lambda_2 \quad \mathbf{A}_{\mp 5} &= -\sqrt{\frac{2}{5}}\frac{\omega_Q}{\omega_1}\hat{T}_{11}(a) + \sqrt{2}\,\hat{T}_{20} \pm \sqrt{\frac{2}{3}}\frac{\lambda_2}{\omega_1}\hat{T}_{21}(s) + \sqrt{\frac{2}{3}}\left(1 - \frac{\omega_Q}{\omega_1}\right)\hat{T}_{22}(s) \\
&\quad + \frac{1}{\sqrt{15}}\left(5 - \frac{2\omega_Q}{\omega_1}\right)\hat{T}_{31}(a) \pm \sqrt{\frac{2}{3}}\frac{\lambda_2}{\omega_1}\hat{T}_{32}(a) + \hat{T}_{33}(a) \qquad [35]
\end{aligned}
$$

With the eigensystem in Eq. [35], the time evolution of the initial single-quantum coherence $\hat{T}_{11}(a)$, in the presence of an on-resonance RF field, takes on the form

$$
\begin{aligned}
e^{iH_S^*t}\hat{T}_{11}(a)e^{-iH_S^*t} &= a_{11}(t)\hat{T}_{11}(a) + a_{20}(t)\hat{T}_{20} \\
&\quad + a_{21}(t)\hat{T}_{21}(s) + a_{22}(t)\hat{T}_{22}(s) + a_{31}(t)\hat{T}_{31}(a) \\
&\quad + a_{32}(t)\hat{T}_{32}(a) + a_{33}(t)\hat{T}_{33}(a) \qquad [36]
\end{aligned}
$$

and the coefficients $a_{ij}(t)$ are set out in Table 1. The spectra resulting from the Fourier transform of the transfer functions pertaining to the evolutions into $\hat{T}_{11}(a)$, $\hat{T}_{20}$, $\hat{T}_{22}(s)$, $\hat{T}_{31}(a)$, and $\hat{T}_{33}(a)$ show a central resonance and two satellite pairs at frequencies λ_1 and λ_2, whereas the contributions related to $\hat{T}_{21}(s)$ and $\hat{T}_{32}(a)$ transform into two satellite pairs in antiphase. Measurement of the positions of the satellites provides the RF power and the static quadrupolar coupling parameter. The satellites are liable to line-broadening effects related to RF field inhomogeneity and, accordingly, the *central* lines in the corresponding spectra are designated for relaxation studies.

The Relaxation Contribution

To calculate the shape of the central lines, we have to incorporate relaxation effects into the differential equations through the addition of the relaxation contribution to the master equation. With the fluctuating quadrupolar interaction in Eq. [5] of part I and the Larmor frequency rotating frame, the relaxation superoperator in Eq. [8] of part I takes on the form

$$
\begin{aligned}
f(\sigma^*) = -(eQ/\hbar)^2 &\sum_{m=-2}^{2} \\
&\times \int_0^\infty [T_{2m}, [\exp(-iH_S^*\tau)T_{2m}^\dagger\exp(iH_S^*\tau), \sigma^*(t)]] \\
&\times \langle [F_{2m}^*(t) - \langle F_{2m}^*\rangle][F_{2m}(t-\tau) - \langle F_{2m}\rangle]\rangle \\
&\times \exp(im\omega_0\tau)d\tau \qquad [37]
\end{aligned}
$$

Table 2 Coefficients Giving the Time Dependence of $\hat{T}_{20}$ Under H_S^*

$a_{11}(t)$	$-\frac{3\omega_1\omega_Q}{2\sqrt{5}}\left(\frac{\cos\lambda_1 t}{\lambda_1^2}+\frac{\cos\lambda_2 t}{\lambda_2^2}-\frac{\lambda_1^2+\lambda_2^2}{\lambda_1^2\lambda_2^2}\right)$
$a_{20}(t)$	$\frac{\omega_Q^4+\omega_1^2\omega_Q^2+4\omega_1^4}{\lambda_1^2\lambda_2^2}+\frac{3\omega_1^2}{2}\left(\frac{\cos\lambda_1 t}{\lambda_1^2}+\frac{\cos\lambda_2 t}{\lambda_2^2}\right)$
$a_{21}(t)$	$-\frac{i\sqrt{3}\,\omega_1}{2}\left(\frac{\sin\lambda_1 t}{\lambda_1}+\frac{\sin\lambda_2 t}{\lambda_2}\right)$
$a_{22}(t)$	$\frac{\sqrt{3}\,\omega_1}{2}\left[\omega_Q\left(\frac{\cos\lambda_1 t}{\lambda_1^2}-\frac{\cos\lambda_2 t}{\lambda_2^2}\right)+\omega_1\left(\frac{\cos\lambda_1 t}{\lambda_1^2}+\frac{\cos\lambda_2 t}{\lambda_2^2}\right)+\frac{2\omega_1}{\lambda_1^2\lambda_2^2}(\omega_Q^2-4\omega_1^2)\right]$
$a_{31}(t)$	$-\frac{\sqrt{3}\,\omega_1}{2\sqrt{10}}\left[2\omega_Q\left(\frac{\cos\lambda_1 t}{\lambda_1^2}+\frac{\cos\lambda_2 t}{\lambda_2^2}\right)+5\omega_1\left(\frac{\cos\lambda_1 t}{\lambda_1^2}-\frac{\cos\lambda_2 t}{\lambda_2^2}\right)-\frac{4\omega_Q}{\lambda_1^2\lambda_2^2}(\omega_Q^2-\omega_1^2)\right]$
$a_{32}(t)$	$\frac{i\sqrt{3}\,\omega_1}{2}\left(\frac{\sin\lambda_1 t}{\lambda_1}-\frac{\sin\lambda_2 t}{\lambda_2}\right)$
$a_{33}(t)$	$-\frac{3\omega_1^2}{2\sqrt{2}}\left(\frac{\cos\lambda_1 t}{\lambda_1^2}-\frac{\cos\lambda_2 t}{\lambda_2^2}+\frac{\lambda_1^2-\lambda_2^2}{\lambda_1^2\lambda_2^2}\right)$

where the evolution of the spin operator $T_{2m}^{\dagger}$ under H_S^* is given by the solution to the differential in Eqs. [31] and [32]. The relaxation contribution reduces to a combination of the spectral densities $J_m(m\omega_0 \pm \lambda_i)$ at a number of frequencies $m\omega_0 \pm \lambda_i$ with $m = 0$, ± 1, ± 2, and λ_i given by Eqs. [33] and [34]. The imaginary part of the spectral density function results in very small, second-order, frequency shifts and a weak coupling of the two sets of differential equations. These dynamic frequency shifts are ignored. In the terms proportional to the spectral densities at approximately one and two times the Larmor frequency, the time-independent Hamiltonian H_S^*, however, can be neglected, because the Larmor frequency ω_0 generally is much larger than any of the frequencies λ_i and, hence, $J_m(m\omega_0 \pm \lambda_i) \approx J_m(m\omega_0) = J_m$ for $m = \pm 1$ and ± 2. The $m = 0$ term is sensitive to slow molecular motion, and the time evolution of the corresponding spin operator T_{20} under the action of H_S^* has to be taken into account explicitly. With the eigensystem in Eq. [35], the evolution of T_{20} ($=2\sqrt{3/2}\ \hat{T}_{20}$) is summarized as

$$e^{iH_S^*t}\hat{T}_{20}e^{-iH_S^*t} = a_{11}(t)\hat{T}_{11}(a) + a_{20}(t)\hat{T}_{20} + a_{21}(t)\hat{T}_{21}(s) + a_{22}(t)\hat{T}_{22}(s) + a_{31}(t)\hat{T}_{31}(a) + a_{32}(t)\hat{T}_{32}(a) + a_{33}(t)\hat{T}_{33}(a) \quad [38]$$

where the coefficients $a_{ij}(t)$ are set out in Table 2. The spin-operator double-commutator now can be calculated with the commutation relationships (*22, 23*), and the relaxation contribution takes on the form (*16, 17*)

$$\frac{d}{dt}\begin{pmatrix}\hat{T}_{11}(a)\\ \hat{T}_{20}\\ \hat{T}_{21}(s)\\ \hat{T}_{22}(s)\\ \hat{T}_{31}(a)\\ \hat{T}_{32}(a)\\ \hat{T}_{33}(a)\end{pmatrix} = -\begin{pmatrix} 3/10D+J_1+2/5J_2 & 0 & 0 & -\sqrt{15}/10E & \sqrt{6}/10D-\sqrt{6}/5J_2 & 0 & 0\\ 3\sqrt{5}/10A & 2J_1+2J_2 & 0 & \sqrt{3}/2B & \sqrt{30}/10A & 0 & 0\\ 0 & 0 & 3/2G+J_1+2J_2 & 0 & 0 & 3/2F & 0\\ 3\sqrt{15}/10F & 0 & 0 & 3/2G+2J_1+J_2 & 3\sqrt{10}/10F & 0 & 0\\ 3\sqrt{6}/20I-\sqrt{6}/5J_2 & 0 & 0 & 3\sqrt{10}/20J & 3/10I+J_1+3/5J_2 & 0 & 0\\ 0 & 0 & 3/2F & 0 & 0 & 3/2G+J_2 & 0\\ 3\sqrt{10}/20B & 0 & 0 & \sqrt{6}/4A & \sqrt{15}/10B & 0 & J_1+J_2 \end{pmatrix}\begin{pmatrix}\hat{T}_{11}(a)\\ \hat{T}_{20}\\ \hat{T}_{21}(s)\\ \hat{T}_{22}(s)\\ \hat{T}_{31}(a)\\ \hat{T}_{32}(a)\\ \hat{T}_{33}(a)\end{pmatrix} \quad [39]$$

and

$$\frac{d}{dt}\begin{pmatrix}\hat{T}_{10}\\ \hat{T}_{11}(s)\\ \hat{T}_{21}(a)\\ \hat{T}_{22}(a)\\ \hat{T}_{30}\\ \hat{T}_{31}(s)\\ \hat{T}_{32}(s)\\ \hat{T}_{33}(s)\end{pmatrix} = -\begin{pmatrix} 2/5J_1+8/5J_2 & 0 & \sqrt{15}/10A & 0 & 4/5J_1-4/5J_2 & 0 & \sqrt{15}/5B & 0\\ 0 & 3/10C+J_1+2/5J_2 & 0 & -\sqrt{15}/10A & 0 & \sqrt{6}/10C-\sqrt{6}/5J_2 & 0 & 0\\ 0 & 0 & 3/2G+J_1+2J_2 & 0 & 0 & 0 & 0 & 0\\ 0 & 0 & 0 & 3/2G+2J_1+J_2 & 0 & 0 & 0 & 0\\ 4/5J_1-4/5J_2 & 0 & \sqrt{15}/5A & 0 & 8/5J_1+2/5J_2 & 0 & -\sqrt{15}/10B & 0\\ 0 & 3\sqrt{6}/20H-\sqrt{6}/5J_2 & 0 & 3\sqrt{10}/20A & 0 & 3/10H+J_1+3/5J_2 & 0 & 0\\ 0 & 0 & 0 & 0 & 0 & 0 & 3/2G+J_2 & 0\\ 0 & 3\sqrt{10}/20B & 0 & \sqrt{6}/4A & 0 & \sqrt{15}/10B & 0 & J_1+J_2 \end{pmatrix}\begin{pmatrix}\hat{T}_{10}\\ \hat{T}_{11}(s)\\ \hat{T}_{21}(a)\\ \hat{T}_{22}(a)\\ \hat{T}_{30}\\ \hat{T}_{31}(s)\\ \hat{T}_{32}(s)\\ \hat{T}_{33}(s)\end{pmatrix} \quad [40]$$

The coefficients A through J are linear combinations of the spectral densities at frequencies λ_1, λ_2, and zero: $J_0(\lambda_1) = J_{\lambda 1}$, $J_0(\lambda_2) = J_{\lambda 2}$, and $J_0(0) = J_0$, respectively. The coefficients of these combinations are collected in Table 3. The frequencies λ_1 and λ_2 are related to both the residual quadrupolar cou-

Table 3 Coefficients in Eqs. [39] and [40] in Terms of the Spectral Densities $J_0(\lambda_1)$, $J_0(\lambda_2)$, and $J_0(0)$

	$J_0(\lambda_1)$	$J_0(\lambda_2)$	$J_0(0)$
A	$\frac{\omega_1(\omega_Q+\omega_1)}{\lambda_1^2}$	$\frac{\omega_1(\omega_Q-\omega_1)}{\lambda_2^2}$	$-\frac{2\omega_1\omega_Q(\omega_Q^2+2\omega_1^2)}{\lambda_1^2\lambda_2^2}$
B	$-\frac{\omega_1(\omega_Q+\omega_1)}{\lambda_1^2}$	$\frac{\omega_1(\omega_Q-\omega_1)}{\lambda_2^2}$	$-\frac{2\omega_1^2(\omega_Q^2-4\omega_1^2)}{\lambda_1^2\lambda_2^2}$
C	$-\frac{\omega_1(\omega_Q-2\omega_1)}{\lambda_1^2}$	$\frac{\omega_1(\omega_Q+2\omega_1)}{\lambda_2^2}$	$\frac{2(\omega_Q^4+8\omega_1^4)}{\lambda_1^2\lambda_2^2}$
D	$\frac{\omega_1(\omega_Q+4\omega_1)}{\lambda_1^2}$	$-\frac{\omega_1(\omega_Q-4\omega_1)}{\lambda_2^2}$	$\frac{2\omega_Q^2(\omega_Q^2+2\omega_1^2)}{\lambda_1^2\lambda_2^2}$
E	$\frac{\omega_1(\omega_Q+4\omega_1)}{\lambda_1^2}$	$\frac{\omega_1(\omega_Q-4\omega_1)}{\lambda_2^2}$	$-\frac{2\omega_1\omega_Q(\omega_Q^2-4\omega_1^2)}{\lambda_1^2\lambda_2^2}$
F	$-\frac{\omega_1^2}{\lambda_1^2}$	$\frac{\omega_1^2}{\lambda_2^2}$	$-\frac{4\omega_1^3\omega_Q}{\lambda_1^2\lambda_2^2}$
G	$\frac{\omega_1^2}{\lambda_1^2}$	$\frac{\omega_1^2}{\lambda_2^2}$	$\frac{2}{3}\left[\frac{\omega_Q^4+\omega_Q^2\omega_1^2+4\omega_1^4}{\lambda_1^2\lambda_2^2}\right]$
H	$\frac{\omega_1(\omega_Q+3\omega_1)}{\lambda_1^2}$	$-\frac{\omega_1(\omega_Q-3\omega_1)}{\lambda_2^2}$	$\frac{2}{3}\left[\frac{2\omega_Q^4+5\omega_Q^2\omega_1^2-4\omega_1^4}{\lambda_1^2\lambda_2^2}\right]$
I	$-\frac{\omega_1(\omega_Q-\omega_1)}{\lambda_1^2}$	$\frac{\omega_1(\omega_Q+\omega_1)}{\lambda_2^2}$	$\frac{2}{3}\left[\frac{2\omega_Q^4-\omega_Q^2\omega_1^2+20\omega_1^4}{\lambda_1^2\lambda_2^2}\right]$
J	$\frac{\omega_1(\omega_Q-\omega_1)}{\lambda_1^2}$	$\frac{\omega_1(\omega_Q+\omega_1)}{\lambda_2^2}$	$-\frac{2\omega_1\omega_Q(\omega_Q^2+6\omega_1^2)}{\lambda_1^2\lambda_2^2}$

pling and the (tunable) RF field strength according to Eq. [33]. Because of the presence of the RF field, the invariance of the spin system under a rotation about the z-axis is lifted. This results in a different relaxation behavior of the symmetric and antisymmetric tensor combination. In the absence of a low-frequency dispersion, i.e., when $J_0 \approx J_{\lambda 1} \approx J_{\lambda 2}$, the ω_Q and ω_1 dependencies in the relaxation in Eqs. [39] and [40] vanish and the matrices reduce to the much simpler forms in terms of J_0, J_1, and J_2 only and are listed in part I. Without RF, the ω_Q-dependence in the rates vanishes, because the static quadrupolar Hamiltonian H^*_{QS} commutes with the $m = 0$ term in the fluctuating quadrupolar Hamiltonian H^*_{QF}. The total time dependence of the basis operators is given by the sums of Eqs. [31] and [39] and Eqs. [32] and [40]. Once the eigenvalues and eigenoperators are known, the time dependence of each of the basis operators can be determined. In the simultaneous presence of an RF field and a static quadrupolar coupling, the master equation can not be solved in analytical form.

Perturbation Analysis of the Line Shapes

Under the condition that the line widths are much smaller than the frequencies λ_1 and λ_2, the operators corresponding to the nonsingular eigenvalues in the eigensystem in Eq. [35] are to a very good approximation still eigenoperators if the relaxation contribution is included. Accordingly, the operators $\mathbf{A}_{\pm 4}$ and $\mathbf{A}_{\pm 5}$ oscillate with frequencies $\pm\lambda_1$ and $\pm\lambda_2$, respectively, and are decoupled and relax independently. The intensities of the corresponding satellite pairs are given by the transfer functions in Table 1. For the corresponding rates R_4 and R_5, the reader is referred to Ref. *18*, but they have little practical value, because of additional broadening effects related to RF field inhomogeneity. The line shape of the central resonance is determined by the relaxation-induced perturbation of the null space spanned by operators $\mathbf{A}_1$, $\mathbf{A}_2$, and $\mathbf{A}_3$ (however, these operators are still decoupled from $\mathbf{A}_{\pm 4}$ and $\mathbf{A}_{\pm 5}$ if the line widths are much smaller than the frequencies λ_1 and λ_2). To obtain the line shape, the corresponding subset of the master equation in the eigenoperator representation in Eq. [35] (the secular terms) has to be diagonalized and subsequently integrated in analytical form. For this purpose, one must solve the secular equation pertaining to the operators $\mathbf{A}_1$, $\mathbf{A}_2$, and $\mathbf{A}_3$ to determine the eigenvalues (relaxation rates) and to calculate the corresponding eigenoperators. The eigenoperators are reported in Ref. *18* and the rates take on the form

$$R_S^{1\rho} = J_1 + J_2, \quad R_{F\mp}^{1\rho} = p \mp \sqrt{q^2 + r^2} \quad [41]$$

with

$$p = \frac{3\omega_1^2}{2}\left(\frac{J_{\lambda 2}}{\lambda_2^2} + \frac{J_{\lambda 1}}{\lambda_1^2}\right) + \frac{3}{2}J_1 + \frac{3(\omega_Q^4 + 2\omega_1^2\omega_Q^2 + 8\omega_1^4)}{2\lambda_1^2\lambda_2^2}J_2$$

$$q = \frac{3\omega_1^2}{2}\left(\frac{J_{\lambda 2}}{\lambda_2^2} - \frac{J_{\lambda 1}}{\lambda_1^2} - \frac{4\omega_Q\omega_1}{\lambda_1^2\lambda_2^2}J_2\right),$$

$$r = \frac{(\omega_Q - 2\omega_1)(\omega_Q + 2\omega_1)}{2\lambda_1\lambda_2}(J_1 + J_2) \quad [42]$$

Because of the 3D null space, the central resonance generally is trimodal and consists of a narrow component related to a slowly relaxing mode and two broad components pertaining to two faster relaxing modes with rates $R_S^{1\rho}$ and $R_{F\mp}^{1\rho}$, respectively. Slow dynamics is probed by the fast modes, because the rates $R_{F\mp}^{1\rho}$ are sensitive to the spectral densities $J_{\lambda 1}$ and $J_{\lambda 2}$ (it should be noticed that they are insensitive to J_0). Furthermore, the rates of the fast modes depend on the relative strengths of the static interactions ω_1/ω_Q, whereas the slow relaxation rate $R_S^{1\rho}$ is sensitive to the high-frequency contributions J_1 and J_2 only.

As far as the *central* line is concerned, the locked $\hat{T}_{11}(a)$ coherence transfers into

$$\hat{T}_{11}(a) \rightarrow g_{11}(t)\hat{T}_{11}(a) + g_{20}(t)\hat{T}_{20} + g_{22}(t)\hat{T}_{22}(s) + g_{31}(t)\hat{T}_{31}(a) + g_{33}(t)\hat{T}_{33}(a) \quad [43]$$

with the relaxation functions

$$g_{ij}(t) = A_S\exp\{-R_S^{1\rho}t\} + A_{F-}\exp\{-R_{F-}^{1\rho}t\} + A_{F+}\exp\{-R_{F+}^{1\rho}t\} \quad [44]$$

Note that the restriction to the central line is at the same level of approximation as the restriction to the nonoscillating, secular terms in the master equation if the time-dependent part of the Hamiltonian is removed by a suitable transformation to an interaction representation. The amplitudes of the slow and fast modes A_S and $A_{F\mp}$, respectively, are calculated with the eigenoperators and have been set out in Table 4. The amplitude of the slow mode does not depend on the spin-lock field strength or the value of the static quadrupolar coupling. For the fast modes, the amplitudes depend on ω_1/ω_Q as well as the spectral densities through the parameters q and r. In particular, the transfers into the quadrupolar spin polarization $\hat{T}_{20}$ and the rank-two double-quantum coherence $\hat{T}_{22}(s)$

Table 4 Amplitudes in the Relaxation Functions of the Central Resonance

	A_S	$A_{F\mp}$
$g_{11}(t)$	$\frac{1}{5}$	$\frac{1}{10}\left[\frac{\omega_Q^4 + 4\omega_Q^2\omega_1^2 + 64\omega_1^4}{\lambda_1^2\lambda_2^2} \pm \left(\frac{6\omega_Q^3\omega_1 q}{\lambda_1^2\lambda_2^2\sqrt{q^2+r^2}} + \frac{(\omega_Q + 4\omega_1)(\omega_Q - 4\omega_1)r}{\lambda_1\lambda_2\sqrt{q^2+r^2}}\right)\right]$
$g_{20}(t)$	0	$\frac{1}{2\sqrt{5}}\left[\frac{3\omega_Q\omega_1(\omega_Q^2 + 4\omega_1^2)}{\lambda_1^2\lambda_2^2} \pm \left(\frac{(\omega_Q^4 - 2\omega_Q^2\omega_1^2 + 16\omega_1^4)q}{\lambda_1^2\lambda_2^2\sqrt{q^2+r^2}} - \frac{3\omega_Q\omega_1 r}{\lambda_1\lambda_2\sqrt{q^2+r^2}}\right)\right]$
$g_{22}(t)$	0	$-\frac{\sqrt{3}}{2\sqrt{5}}\left[\frac{\omega_Q\omega_1(\omega_Q^2 - 4\omega_1^2)}{\lambda_1^2\lambda_2^2} \pm \left(\frac{2\omega_1^2(\omega_Q^2 + 8\omega_1^2)q}{\lambda_1^2\lambda_2^2\sqrt{q^2+r^2}} + \frac{\omega_Q\omega_1 r}{\lambda_1\lambda_2\sqrt{q^2+r^2}}\right)\right]$
$g_{31}(t)$	$-\frac{\sqrt{3}}{5\sqrt{2}}$	$-\frac{\sqrt{3}}{10\sqrt{2}}\left[\frac{(\omega_Q^4 - 6\omega_Q^2\omega_1^2 - 16\omega_1^4)}{\lambda_1^2\lambda_2^2} \pm \left(\frac{\omega_Q\omega_1(\omega_Q^2 + 20\omega_1^2)q}{\lambda_1^2\lambda_2^2\sqrt{q^2+r^2}} + \frac{(\omega_Q^2 + 4\omega_1^2)r}{\lambda_1\lambda_2\sqrt{q^2+r^2}}\right)\right]$
$g_{33}(t)$	$\frac{1}{\sqrt{10}}$	$-\frac{1}{2\sqrt{10}}\left[\frac{\omega_Q^4 - 2\omega_Q^2\omega_1^2 + 16\omega_1^4}{\lambda_1^2\lambda_2^2} \pm \left(\frac{3\omega_Q\omega_1(\omega_Q^2 + 4\omega_1^2)q}{\lambda_1^2\lambda_2^2\sqrt{q^2+r^2}} + \frac{(\omega_Q + 2\omega_1)(\omega_Q - 2\omega_1)r}{\lambda_1\lambda_2\sqrt{q^2+r^2}}\right)\right]$

are bimodal, i.e., $g_{20}(t)$ and $g_{22}(t)$ do not exhibit a slow mode ($A_S = 0$). In the limit $\omega_1 \gg \omega_Q$, the RF field strength far exceeds the static quadrupolar coupling and the frequencies collapse to the same value of $\lambda_1 = \lambda_2 = 2\omega_1$. For a such strong RF field, the rank-two $\hat{T}_{22}(s)$ and $\hat{T}_{20}$ coherences are no longer excited and the evolution into the other coherences reduces to the one for $\omega_Q = 0$ as given in Eq. [12]. Rank-two coherences are excited only when there are residual quadrupolar couplings in the sample and provided the spin-lock field strength is comparable with these couplings. Hence, a spin-lock pulse sequence followed by a coherence transfer pulse cycled through the $\hat{T}_{22}(s)$ or $\hat{T}_{20}$ state is selective to nuclei in an ordered environment, like the double-quantum magic-angle and the Jeener-Broekaert pulse sequences as reviewed in part I (*5*).

Pulse Sequences

First, we will discuss the conventional spin-lock experiment, in which the signal is sampled directly after the spin-lock field has been switched off. The detected signal is proportional to the $\hat{T}_{11}(a)$, $\hat{T}_{21}(s)$, and $\hat{T}_{31}(a)$ single-quantum coherence contributions. After 2D Fourier transformation, the central resonance in the F_1 domain (i.e., the nonoscillating and secular contribution) contains the contributions from $\hat{T}_{11}(a)$ and $\hat{T}_{31}(a)$ only; the contribution related to $\hat{T}_{21}(s)$ transforms into two satellite pairs in antiphase and can be spread out over a large frequency range. Hence, the directly detected signal pertaining to the central resonance in F_1 takes the form

$$s(t_1, t_2) = g_{11}(t_1) f_{11}^{(1)}(t_2) + g_{31}(t_1) f_{13}^{(1)}(t_2) \quad [45]$$

To identify the $T_{1\rho}$ relaxation of the satellites and central transition, the evolution functions in the detection period in Eq. [47] of part I are expanded and the signal is expressed as

$$s(t_1, t_2) = \frac{1}{5}\left[(3g_{11}(t_1) + \sqrt{6}\, g_{31}(t_1)) \times \cos(\omega_Q t_2)\exp(-R_s t_2) + (2g_{11}(t_1) - \sqrt{6}\, g_{31}(t_1))\exp(-R_c t_2)\right] \quad [46]$$

where $R_s = J_0 + J_1 + J_2$ and $R_c = J_1 + J_2$ are the transverse relaxation rates of the satellites and the central resonance (without spin-lock field), respectively. The signals in the F_1 domain, pertaining to a certain value of the static quadrupolar interaction, can be selected by taking a section along F_1 at the position of the corresponding satellite signal in F_2. The contributions pertaining to the satellites and central transition in F_2 are identified easily in the first and the second term on the right side of Eq. [46], respectively. For the satellites, the amplitude of the slow mode A_S vanishes in the relevant combination of the relaxation functions $3g_{11} + \sqrt{6}g_{31}$ (see Table 4). Accordingly, the $T_{1\rho}$ relaxation of the satellites is bimodal and is particularly sensitive to slow dynamics. However, the latter relaxation becomes *single* exponential if the RF field strength far exceeds the static quadrupolar coupling $\omega_1 \gg \omega_Q$. In this limiting situation, $A_{F+} = 0$ for all coherences and the spin-lock relaxation rate of the satellites takes the simple form

$$R_{F-}^{1\rho} = \frac{3}{4} J_{\lambda 1} + J_1 + \frac{1}{4} J_2 \quad (\omega_1 \gg \omega_Q,\ \lambda_1 = 2\omega_1) \quad [47]$$

The spin-polarization quadrupolar order $\hat{T}_{20}$, the double-quantum coherences $\hat{T}_{22}(s)$ and $\hat{T}_{32}(a)$, or the triple-quadrupolar coherence $\hat{T}_{33}(a)$ can be monitored if the spin-lock sequence is followed by a coherence transfer pulse

$$\pi/2(\phi) - B_1(\phi + 90),\ t_1 - \beta(\phi') - \text{acquire},\ t_2 \qquad [48]$$

where the phase ϕ and the flip angle β have to be specified to select the desired coherence order. The other coherences belong to the other subset and are irrelevant in the context of the spin-lock experiment (they also do not exhibit a central line in the F_1 domain).

Cycling through the $\hat{T}_{20}$ state has proven to be most suitable to extract dynamic information in the presence of static quadrupolar interactions because the corresponding relaxation function $g_{20}(t_1)$ does not exhibit a slow mode and the pulse sequence is selective to nuclei in an anisotropic environment (*3*). For optimized detection of $\hat{T}_{20}$, the flip angle of the final coherence transfer pulse should be $\beta = 45°$. The phase ϕ is stepped through 0, 90, 180, and 270° while the receiver phase is kept at a constant value. Because of the invariance of $\hat{T}_{20}$ with respect to a rotation about the z-axis, the value of the phase ϕ' is irrelevant. Because of pulse imperfections, Zeeman order $\hat{T}_{10}$ and octopolar spin polarization $\hat{T}_{30}$ also may be excited. However, their signal contributions can be suppressed by performing two experiments with coherence transfer pulse angles $\beta = 45$ and 135°, respectively, and subsequent subtraction of the resulting spectra. For a single-pulse angle, the same effect can be achieved if one takes the difference of the sections at the resonance positions of the two satellites in the acquisition domain. The final pulse transfers the quadrupolar spin polarization $\hat{T}_{20}$ created under the lock into second-rank single-quantum coherence $\hat{T}_{21}(s)$, which evolves into detectable transverse magnetization during the detection time t_2. Including the satellites at frequencies λ_1 and λ_2, the signal reads

$$s(t_1, t_2, p = 0) = \left[g_{20}(t_1) - \frac{3\omega_Q\omega_1}{2\sqrt{5}} \left(\frac{\cos(\lambda_1 t_1)\exp(-R_4 t_1)}{\lambda_1^2} + \frac{\cos(\lambda_2 t_1)\exp(-R_5 t_1)}{\lambda_2^2} \right) \right] f_{12}^{(1)}(t_2) \qquad [49]$$

with the evolution into the *central* resonance in F_1 given by $g_{20}(t_1)$ in Table 4. For the rates of the satellites, Ref. *18* may be consulted, but they have little practical value because of broadening effects related to RF field inhomogeneity. The signal is identically zero if there is no quadrupolar coupling, as well as in the case $\omega_Q \neq 0$, but if $\omega_1 \gg \omega_Q$ or $\omega_Q \gg \omega_1$. Therefore, signal is only observed in the presence of a static quadrupolar coupling and provided $\omega_Q \approx \omega_1$.

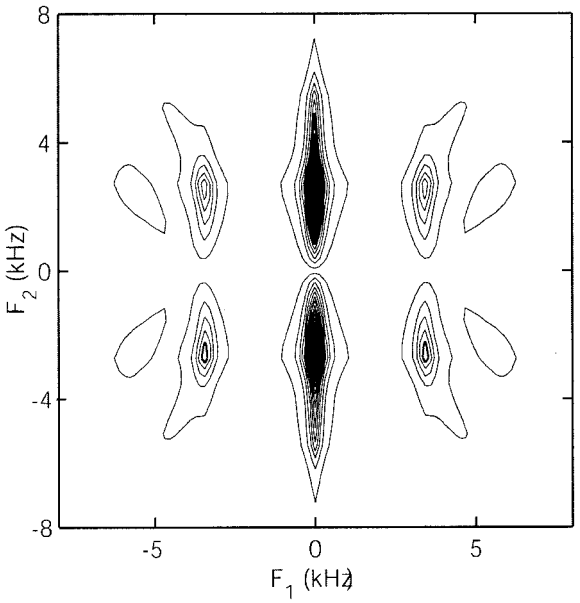

Figure 2 Simulated 2D power spectrum of the selectively detected quadrupolar order $\hat{T}_{20}$. The absolute value of the spectrum is displayed. Spin-lock field strength: $\omega_1/2\pi = 1.95$ kHz; maximum quadrupolar splitting measured along the local director $\bar{\omega}_Q/2\pi = 5.4$ kHz.

A simulated 2D contour spectrum, pertaining to a spin-lock experiment cycled through the $\hat{T}_{20}$ state, is shown in Fig. 2. The spectrum represents a powder average over randomly oriented domains and all of the domains have the same dynamical properties. Furthermore, the spectrum was calculated for a moderate RF field strength $\omega_1/2\pi = 1.95$ kHz and the values of the other parameters were chosen in accordance with the experimental results for sodium in Xanthan liquid crystal (*3*). Note that the phase information is lost, because the absolute value of the spectrum is displayed. Figure 3 shows a slice along F_2 at $F_1 = 0$, which represents a powder average of the satellite pair in antiphase with maximum splitting $\bar{\omega}_Q/2\pi = 5.4$ kHz. A slice along F_1 at $\omega_1/2\pi = 1.95$ kHz in F_2 is displayed in Fig. 4. This slice pertains to those domains in the powder with a splitting just matching the spin-lock field strength: $\omega_Q/2\pi = \omega_1/2\pi = 1.95$ kHz. Apart from the central resonance, the spectrum displays the two characteristic satellite pairs at frequencies $\lambda_1/2\pi$ and $\lambda_2/2\pi$. The central line is com-

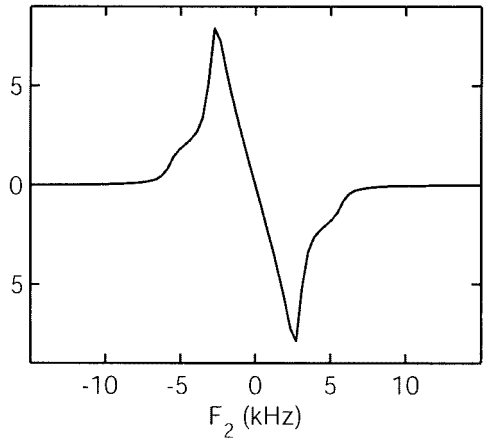

Figure 3 Simulated slice along F_2 (at $F_1 = 0$) of the selectively detected $\hat{T}_{20}$ coherence in Fig. 2.

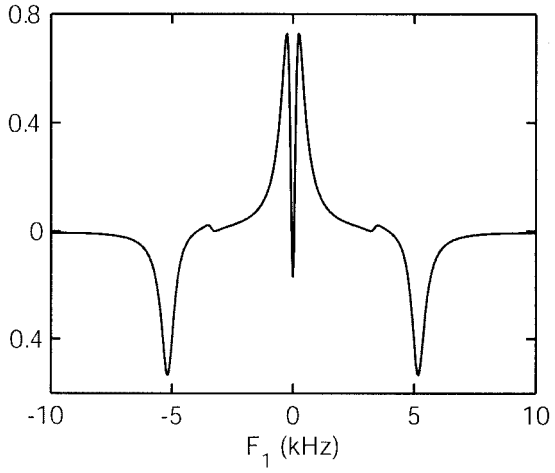

Figure 5 Simulated slice as in Fig. 4, but for the double-quantum $\hat{T}_{22}(s)$ coherence.

posed of a sum of two Lorentzians with amplitudes and rates depending on ω_1, ω_Q, and the spectral densities $J_{\lambda 1}$, $J_{\lambda 2}$, J_1, and J_2 (it does not exhibit a slow mode). The high-frequency contributions J_1 and J_2 can be obtained from an inversion recovery experiment, leaving $J_{\lambda 1}$ and $J_{\lambda 2}$ to be determined from a fit of the Fourier transform of $g_{20}(t_1)$ to the central line. In practice, it may be difficult to fit $J_{\lambda 1}$ and $J_{\lambda 2}$, despite the bimodal line shape. However, numerical evaluation of $g_{20}(t_1)$ shows that the dependence of the line shape on $J_{\lambda 2}$ is minor but not negligible for $\omega_Q \approx \omega_1$. For instance, in the average rate pertaining to g_{20}, which corresponds to the first cumulant, the dependence on $J_{\lambda 2}$ vanishes for $\omega_Q = \omega_1$. Accordingly, it is advisable to perform experiments with various spin-lock field strengths, extract spectra in F_1 for which the condition $\omega_Q = \omega_1$ is satisfied (as in Fig. 4), and optimize the dominant spectral density $J_{\lambda 1}$ in an iterative manner (*3*).

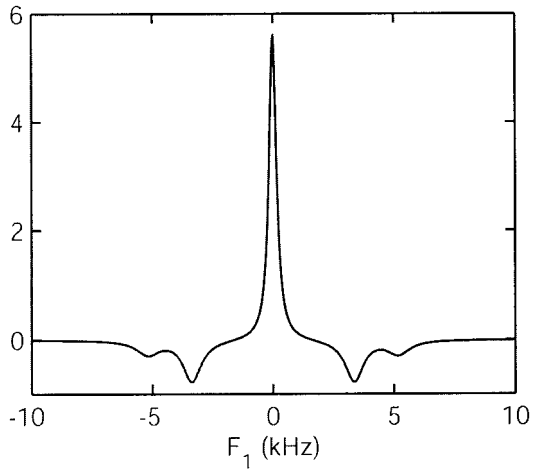

Figure 4 Simulated slice along F_1 of the selectively detected $\hat{T}_{20}$ coherence in Fig. 2. The section at $F_2 = \omega_1/2\pi = 1.95$ kHz is displayed. Accordingly, the spectrum pertains to those domains in the powder with a splitting that just matches the spin-lock strength.

In the double-quantum filtration experiment, the phase ϕ is stepped through the values 0, 90, 180, and 270°, while the receiver phase is alternated between 0 and 180°. The phase ϕ' is set to 45° for selective, simultaneous, detection of $\hat{T}_{22}(s)$ and $\hat{T}_{32}(a)$ (the other combinations are selectively detected if $\phi' = 0°$). A double-quantum filtered 2D spectrum with coherence transfer pulse angle $\beta = 90°$ shows two signal contributions; $\hat{T}_{22}(s)$ and $\hat{T}_{32}(a)$. The latter contribution does not exhibit a central resonance in F_1 and, hence, is irrelevant from a relaxation analysis point of view. However, the $\hat{T}_{32}(a)$ coherence contribution can be suppressed [at the cost of signal-to-noise ratio (S/N) ratio] by decreasing the length of the final coherence transfer pulse so that $\beta = \arccos(1/\sqrt{3}) = 54.7°$. In the latter situation, the relevant bimodal relaxation function describing the evolution of the central line under the lock is $g_{22}(t_1)$. A simulated spectrum pertaining to the $\hat{T}_{22}(s)$ coherence is shown in Fig. 5. Note the characteristic line shape of the bimodal central resonance; the amplitudes of the fast modes have opposite signs (*18*).

In the triple-quantum filtration experiment, the optimized pulse angle $\beta = 90°$ and the phase ϕ is stepped through the values 30, 90, 150, 210, 270, and 330°, while the receiver phase is toggled between 0 and 180° for consecutive scans. Here, the phase ϕ' of the final pulse is set to 0° for selective detection of $\hat{T}_{33}(a)$ [the experiment is optimized for the unwanted $\hat{T}_{33}(s)$ coherence if $\phi' = 30°$; $\hat{T}_{33}(s)$ belongs to the other subset and

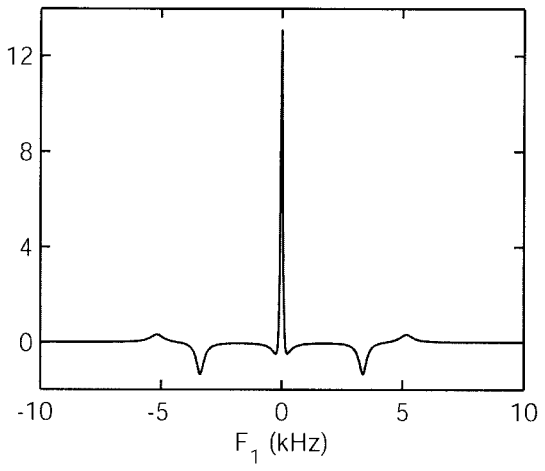

Figure 6 Simulated slice as in Fig. 4, but for the triple-quantum $\hat{T}_{33}(a)$ coherence.

does not exhibit a central line]. The relevant evolution function is $g_{33}(t_1)$, which exhibits two fast modes and a slow mode as in the case of the $T_{1\rho}$ experiment without coherence transfer. Because of the presence of the prominent narrow component in the corresponding spectrum (see Fig. 6), the triple-quantum filtration experiment is less eligible to extract dynamic information. Furthermore, it is selective for nuclei involved in slow molecular motion but does not discriminate between nuclei in an isotropic and anisotropic environment.

The preparation of the density operator depends on the RF field strength of the initial pulse. A pure $\hat{T}_{11}(a)$ initial state can be prepared only if the effects of relaxation and the static quadrupolar interaction can be neglected during a sufficiently hard preparation pulse. If this can not be realized experimentally, the initial density operator after the phase shift will be in a mixed state including $\hat{T}_{10}$, $\hat{T}_{30}$, $\hat{T}_{11}(a)$, $\hat{T}_{21}(s)$, $\hat{T}_{22}(s)$, $\hat{T}_{31}(a)$, $\hat{T}_{32}(a)$, and $\hat{T}_{33}(a)$ coherences. The subsequent relaxation of the central resonance under the RF lock is still given by the rates in Eqs. [39] and [40], but the amplitudes of the various modes will be different from those collected in Table 4. Although the amplitudes can be derived analytically, it is more convenient to calculate them with a numeric integration of the master equation (including the effects of the preparation and coherence transfer pulses and the phase shifts). However, it has been checked that under any circumstances the evolutions into $\hat{T}_{20}$ and $\hat{T}_{22}(s)$ coherences do not exhibit a slow mode and remain bimodal.

CONCLUSIONS

The relaxation dynamics of a system of spin 3/2 under strong, on-resonance RF irradiation and in the presence of fluctuating and static quadrupolar interactions was reviewed. For isotropic systems, we also have discussed the dynamics under off-resonance spin-locking conditions and in the Ostroff-Waugh multiple-pulse experiment. In isotropic systems and with a Wigner transformation to an interaction representation in which the time-dependent RF part of the Hamiltonian is removed, it was shown that the spin dynamics under (pulsed) locking conditions is similar to longitudinal relaxation in the rotating frame but with modified relaxation rates. Outside the extreme narrowing limit, the relaxation is biexponential and the fast mode is sensitive to the spectral density on the order of the spin-lock frequency or the pulse cycle time in the case of pulsed RF irradiation. Furthermore, triple-quantum coherences are excited under the lock, which can be monitored with an additional coherence transfer pulse at the end of the spin-lock period. In the presence of static quadrupolar interactions, the external parts of the Hamiltonian can not be removed by a Wigner transformation and the effects of relaxation were treated as a first-order perturbation to the static Hamiltonian. The spectra resulting from Fourier transformation of the evolutions of the on-resonance, spin-locked magnetization into the various coherences display two pairs of satellites and, in some cases, a central line. From the perturbation analysis, it follows that the central line generally is trimodal, consisting of a narrow component related to a slowly relaxing mode and two broad components pertaining to two faster relaxing modes. Neither the amplitude nor the width of the narrow component is affected by the magnitude of the static coupling, whereas the characteristics of the broad components depend in a rather complicated manner on the relative strengths of the static interactions. The evolutions into the spin-polarization quadrupolar order and the rank-two double-quantum coherence do not exhibit a slow mode and are particularly sensitive to slow molecular motion. Furthermore, these coherences can be excited only in the presence of a static coupling and this makes it possible to discern nuclei in an anisotropic environment from those in an isotropic environment.

The application of a spin-lock field for the investigation of molecular dynamics presents several advantages over the conventional sequences as reviewed in part I. Although transverse relaxation gives access to the spectral density at zero frequency only, slow dynamics is probed more efficiently by applying a lock through an RF field covering the kilohertz frequency range. For small splittings or in the presence of a powder-type variation of the static quadrupolar interaction through the sample, the determination of the width of the satellite signals by the conventional

sequences becomes problematic, if not impossible. Here, the spin-lock sequence and its variants come to the rescue and can give valuable information about slow dynamics, which otherwise can not be obtained. Furthermore, the spin-lock sequence has proven to be more efficient than the conventional pulse sequences in generating an observable signal from ions in anisotropic media in both biological tissue and ordered complex fluids.

REFERENCES

1. Woessner DE. 2001. NMR relaxation of spin-3/2 nuclei: Effects of structure, order, and dynamics in aqueous heterogeneous systems. Concepts Magn Reson 13: 294–325.
2. Porion P, Al Muhktar M, Meyer S, Faugère AM, van der Maarel JRC, Delville A. 2001. Nematic ordering of suspensions of charged anisotropic colloids detected by ^{23}Na nuclear magnetic resonance. J Phys Chem B 105: 10505–10514.
3. van der Maarel JRC, Woessner DE, Merritt ME. 2002. Extremely slow counterion dynamics in Xanthan liquid crystal through ^{23}Na and ^{14}N NMR. J Phys Chem B 106:3864–3871.
4. Hancu I, Boada FE, Shen GX. 1999. Three-dimensional triple-quantum-filtered Na-23 imaging of in vivo human brain. Magn Reson Med 42:1146–1154.
5. Hancu I, van der Maarel JRC, Boada FE. 2002. Detection of sodium ions in anisotropic environments through spin-lock NMR. Magn Reson Med 47:68–74.
6. Landau LD, Lifshitz EM. 1977. Quantum mechanics (non-relativistic theory), course of theoretical physics, Vol. 3, 3rd ed. Oxford: Pergamon Press p 133–142.
7. Haeberlen U, Waugh JS. 1969. Spin-lattice relaxation in periodically perturbed systems. Phys Rev 185:420–429.
8. Blicharski JS. 1972. Nuclear magnetic relaxation in the rotating frame. Acta Phys Polon A 41:223–236.
9. Rose ME. 1957. Elementary theory of angular momentum. New York: Wiley.
10. van der Maarel JRC. 1989. Relaxation of spin $S = 3/2$ in the doubly rotating tilted frame. J Chem Phys 91: 1446–1450.
11. Desvaux H, Berthault P. 1999. Study of dynamic processes in liquids using off-resonance rf irradiation. Prog Nucl Magn Reson Spectr 35:295–340.
12. Ernst RR, Bodenhausen G, Wokaun A. 1987. Principles of nuclear magnetic resonance in one and two dimensions. Oxford: Clarendon p 340–341.
13. Ostroff ED, Waugh JS. 1966. Multiple spin echoes and spin locking in solids. Phys Rev Lett 16:1097–1098.
14. van der Maarel JRC. 1991. Relaxation of spin quantum number $S = 3/2$ by multiple-pulse quadrupolar echoes. J Chem Phys 94:4765–4775.
15. van der Maarel JRC, Tromp RH, Leyte JC, Hollander JG, Erkelens C. 1990. Spin $S = 3/2$ $T_{1\rho}$ relaxation; the excitation of the triple-quantum coherences. Chem Phys Letters 169:585–590.
16. van der Maarel JRC. 1993. The relaxation dynamics of spin $I = 1$ nuclei with a static quadrupolar coupling and a radio frequency field. J Chem Phys 99:5646–5653.
17. Hancu I, van der Maarel JRC, Boada FE. 2000. A model for the dynamics of spins 3/2 in biological media: Signal loss during radio frequency excitation in triple-quantum-filtered sodium MRI. J Magn Reson 147:179–191.
18. van der Maarel JRC, Jesse W, Hancu I, Woessner DE. 2001. Dynamics of spin $I = 3/2$ under spin-locking conditions in an ordered environment. J Magn Reson 151:298–313.
19. Wokaun A, Ernst RR. 1977. Selective excitation and detection in multilevel spin systems: Application of single transition operators. J Chem Phys 67:1752–1758.
20. Pandey L, Towta S, Hughes DG. 1986. NMR pulse response and measurement of the quadrupolar coupling constant of $I = 3/2$ nuclei. J Chem Phys 85:6923–6927.
21. Campolieti G, Sanctuary BC, Cole HBR. 1990. Multipole theory of soft pulses in NMR of quadrupolar solids. J Magn Reson 88:457–472.
22. Bowden GJ, Hutchison WD. 1986. Tensor operator formalism for multiple-quantum NMR. 1. Spin-1 nuclei. J Magn Reson 67:403–414.
23. Bowden GJ, Hutchison WD, Khachan J. 1986. Tensor operator formalism for multiple-quantum NMR. 2. Spins 3/2, 2, and 5/2 and general I. J Magn Reson 67:415–437.

BIOGRAPHY

Johan van der Maarel was born in 1960 in Maassluis, The Netherlands. He received his Ph.D. in physical chemistry from Leiden University in 1987. His doctoral work was on the structure and dynamics of water and aqueous solutions. Since then, he has been employed as a Lecturer in Physical and Macromolecular Chemistry and has spent a sabbatical as visiting professor at the University of Minnesota, USA. His research is concerned with the nuclear magnetic resonance technique, but he also applies scattering methods to complex fluid systems. He has been performing studies of polyelectrolytes, polyelectrolyte diblock copolymer micelles, and mesostructures of DNA.